AD-A276 260

OFFICE OF NAVAL RESEARCH

Grant No. _______

R&T Code N00014-92-C-0173

Technical Report #08

INTERACTION OF WATER WITH METAL SURFACES

by

Sheng-Bai Zhu
Michael R. Philpott

Prepared for publication

in the

Journal of Chemical Physics

IBM Research Division, Almaden Research Center,
650 Harry Road, San Jose, CA 95120-6099

1994

Best Available Copy

SECURITY CLASSIFICATION OF THIS PAGE *(When Data Entered)*

REPORT DOCUMENTATION PAGE		READ INSTRUCTIONS BEFORE COMPLETING FORM
1. REPORT NUMBER 08 Technical Report 16	2. GOVT ACCESSION NO.	3. RECIPIENT'S CATALOG NUMBER
4. TITLE *(and Subtitle)* Interaction of Water with Metal Surfaces		5. TYPE OF REPORT & PERIOD COVERED Technical Report
		6. PERFORMING ORG. REPORT NUMBER
7. AUTHOR(s) Sheng-Bai Zhu, Michael R. Philpott		8. CONTRACT OR GRANT NUMBER(s) N00014-92-C-0173
9. PERFORMING ORGANIZATION NAME AND ADDRESS IBM Research Division, Almaden Research Center 650 Harry Road San Jose, CA95120-6099		10. PROGRAM ELEMENT, PROJECT, TASK AREA & WORK UNIT NUMBERS
11. CONTROLLING OFFICE NAME AND ADDRESS Office of Naval Research 800 North Qunicy Street Arlington, VA 22217		12. REPORT DATE 2/18/94
		13. NUMBER OF PAGES 29
14. MONITORING AGENCY NAME & ADDRESS *(If different from Controlling Office)* Dr. Ronald A. De Marco Office of Naval Research, Chemistry Division 800 N. Quincy Street Arlington, VA 22217 U.S.A.		15. SECURITY CLASS *(of this report)* Unclassified
		15a. DECLASSIFICATION/DOWNGRADING SCHEDULE

16. DISTRIBUTION STATEMENT *(of this Report)*

Approved for public release; unlimited distribution.

17. DISTRIBUTION STATEMENT *(of the abstract entered in Block 20, if different from Report)*

Approved for public release; unlimited distribution.

18. SUPPLEMENTARY NOTES

Prepared for publication in the Journal of Chemical Physics

19. KEY WORDS *(Continue on reverse side if necessary and identify by block number)*

20. ABSTRACT *(Continue on reverse side if necessary and identify by block number)*

SEE NEXT PAGE

A new class of potential suitable for modeling the adsorption of water on different metal sites is described. The new potentials are simple in form and convenient for use in computer simulations. In their real space form they comprise three parts: a pair-wise sum of spatial anisotropic 12-6 potentials, a pair-wise sum of isotropic short range potentials, and an image potential. Two modifications of the potential are developed. In the first, the anisotropic potential acts only on the oxygen atom and not on the protons. In the second, the potential acts on all the atoms of the water molecule. In practical calculations it is convenient to transform the potential to a reciprocal space form in the manner described by Steele [Surf. Sci. 36, 317 (1973)]. Adsorption of water at top, bridge, and hollow sites on (100), (110), and (111) surfaces of Pt, Ni, Cu, and Al were studied using two fitting parameters and the results compared with previous theoretical calculations.

Interaction of Water with Metal Surfaces

Sheng-Bai Zhu and Michael R. Philpott
IBM Research Division
Almaden Research Center
San Jose, CA 95120-6099

November 17, 1993

Abstract

A new class of potential suitable for modeling the adsorption of water on different metal sites is described. The new potentials are simple in form and convenient for use in computer simulations. In their real space form they comprise three parts: a pair-wise sum of spatial anisotropic 12-6 potentials, a pair-wise sum of isotropic short range potentials, and an image potential. Two modifications of the potential are developed. In the first, the anisotropic potential acts only on the oxygen atom and not on the protons. In the second, the potential acts on all the atoms of the water molecule. In practical calculations it is convenient to transform the potential to a reciprocal space form in the manner described by Steele [Surf. Sci. 36, 317 (1973)]. Adsorption of water at top, bridge, and hollow sites on (100), (110), and (111) surfaces of Pt, Ni, Cu, and Al were studied using two fitting parameters and the results compared with previous theoretical calculations.

1 Introduction

Understanding the properties and dynamic behavior of water in the vicinity of metallic surfaces is of fundamental importance in electrochemistry, catalysis, and the study of corrosion. A variety of experimental techniques exist capable of providing data about surface water, for example those described in the review of Thiel and Madey [1], surface infrared spectroscopy by O'Grady [2] and Melendres [3], and the X-ray technique described by Toney and coworkers [4]. Computer simulations play an important role by providing detailed microscopic insight about the water multilayers, which is currently unavailable from laboratory experiments. A matter of primary importance for performing a computer simulation is, of course, the knowledge of the relevant interactions. Our purpose in this paper is to describe a new simple potential function useful for molecular dynamics simulations of metal-aqueous interfaces. The weight of experimental and theoretical evidence to be surveyed briefly later, supports the adsorption of water with oxygen atom down on the top site of a metal surface. In contrast a pairwise sum of 12-6 Lennard-Jones (LJ) potentials predicts the binding energy order for adsorption as hollow > bridge > top sites. It is also clear that the electronic properties of the metal play a critical role in the interaction with water which is weakly chemisorbed rather than physisorbed, and that the chemisorption bond directs adsorption to the top site. The key idea in our development is the introduction of a simple angular dependence into the traditional 12-6 Lennard-Jones potential to mimic the directionality of the chemisorptive bond.

In the earliest studies the water-surface potential was assumed to have two components, image terms to describe the polarization interaction of molecular charge with the conduction electrons and 12-6 Lennard-Jones terms to account for Pauli repulsion and the dispersion attraction interaction with all electrons in the core and conduction band. We will refer to this latter part as the core term. Earlier efforts [5, 6, 7, 8] described the interaction of a molecule and the conduction electrons of a metal often by truncating the image potential to the nearest term. In practical computations, the core potential part often appears in its integrated form which, within the first order approximation, is a 10-4 or 9-3 potential. These models, though intuitive, fail to predict orientational properties of water molecules chemisorbed on the surface of a transition metal. Existing experimental data [1] for the work function change suggest that the water dipoles tend to orient perpendicular to the surface rather than parallel to it. In the case of low index faces where the metal atoms are explicitly taken into account, the above mentioned water-wall potential leads to a conclusion that the preferred adsorption is on the hollow sites of the surface [5]. This contradicts the weight of evidence that an adsorption on top of the metal atom is the preferred site, as indicated by both the experimental observations [9] and the quantum mechanical calculations [10, 11, 12, 13, 14]. It is therefore a challenge to find a water-metal surface potential function that is simple in form and still describes the observed preferences.

Extended Hűckel molecular orbital calculations of a water molecule on top of a cluster of five platinum atoms [10] were used by Spohr and Heinzinger [15] and Spohr [16] to fit the water-surface potential to a set of exponential functions. Berkowitz and co-workers [17, 18] have prescribed potential functions for water-Pt(100) and water-Pt(111) interfaces based on the Heinzinger-Spohr form, but incorporating the lattice symmetry and corrugation explicitly. These potentials usefully describe the chemisorption bonding, but not the image contribution or it's contribution to long range interfacial electric fields. In a quite separate approach Siepmann and Sprik [19] have modified the bond-angle-dependent potentials developed for covalent solids [20] by the use of overlapping Gaussian charge distributions centered at the metal atoms, as a compromise between the image charge formalism and a microscopic description of the electronic structure. These more complicated potential models are in qualitative agreement with more elaborate *ab initio* calculations and existing experimental data.

2 Potential Energy Function

The physisorption of molecules on insulators has been usefully modeled in many cases using a pair-wise sum of atom-atom Lennard-Jones 12-6 potentials and r^{-1} Coulomb potentials. The extension of this model to a metal would describe the molecule-core electron interaction with a Lennard-Jones (LJ) potential and the molecule-conduction electron interaction with an image potential. In practice the Lennard-Jones potential also includes Pauli repulsion and attractive dispersion interactions for all the electrons making up the metal. This does not work for water, or for that matter the adsorption of Xe atoms on Pt [21]. Many-body effects other than those giving the asymptotic image interaction are expected to be important for the adsorption on metals. It is not correct to treat metal surface as a simple assembly of uncorrelated atoms, nonadditive interactions should be incorporated. However, to obtain a concise potential in a form which is convenient for adjusting parameters to be useful in computer simulations, it would be very helpful if one could treat the many-body contribution in an approximate but effective manner. In this section, we show that this possibility indeed exists. Introducing angular dependence into the traditional LJ potential can make the top site most favored for a water molecule in an oxygen down geometry.

The two potentials described below are labeled A1 and A2. The later being the all atom model. In both there is an LJ potential modified by incorporation of angular dependence. Instead of spherical symmetry, the repulsive and attractive parts have the symmetry of an ellipsoid of revolution. Several interactions contribute to angular dependent terms: first is the chemisorptive bond interaction involving mixing of orbitals from the metal and oxygen, another comes from the interaction between the permanent dipole moment of the adsorbed molecule and the induced moment of the solid atom [22]. Repulsions due to overlap of electron clouds at short separations are also considered in this modification. In addition, extra terms proportional to r^{-n} are introduced to mimic short-range bonding that pulls the oxygen atom closer to the top atom. These angular dependent, short-range interactions allow better modeling of the adsorption of water on metal surfaces. In simulations where metal atom dynamics and surface reconstruction are not considered, it is useful to explicitly incorporate surface lattice translational symmetry using the method first proposed by Hove and Krumhansl [23] and subsequently universally adopted [24, 25].

In both models, the potential for one molecule interacting with the metal is written

$$V_{w-met} = V_{w-cond} + V_{w-core} \tag{1}$$

where the first term represents the water molecule-conduction electron potential and the second term the molecule-core electron contribution. As usual, we approximate the first term by a classical image potential. The image charge q_{image} of a classical point charge q is located at the symmetrical position below the image plane and has the magnitude [26]

$$q_{\text{image}} = \frac{1-\epsilon_r}{1+\epsilon_r} q \tag{2}$$

The 'correct' choice of the image plane position has been the subject of much debate. It is not deeper into the metal than the first nuclear plane for low index faces. This is the position we will assume. For a grounded ideal metal, the relative permittivity ϵ_r is finite, and $q_{\text{image}} = -q$. For a molecule modeled by point sites, each point charge interacts with all the image charges by means of a Coulomb potential

$$V_{w-cond} = \sum_{l,k} \frac{q_l q_k}{r_{lk}} \tag{3}$$

where the index l stands for the real charge and k for the image charge with r_{lk} being their distance apart. Since the polarization response of the surface changes with the addition of new molecules, Eq. (3) describes a non-additive surface polarization.

The second term in Eq. (1) contains the anisotropic short range potential and the short range r^{-n} potential (n integer) and so requires much more detailed description.

$$V_{w-core} = V_{w-an} + V_{w-isr} \tag{4}$$

where V_{w-isr} is the isotropic short range part and V_{w-an} contains the anisotropic part. Next we construct both these parts separately using pair-wise sums and then use translational symmetry to reduce them to usable forms. Henceforth we drop explicit reference to water (label w)

To begin, consider a perfect crystal surface in which the basic vectors of the lattice are $\mathbf{a}_1$ and $\mathbf{a}_2$. Next consider a point particle p at $\mathbf{r}_p$=(ρ_p, z_p) where z_p is the perpendicular distance above the surface and ρ_p is the projection of $\mathbf{r}_p$ onto the surface plane. The label p stands for O or either of two H atoms. For convenience we choose the x-axis to be parallel to $\mathbf{a}_1$ and take origin to be at the inversion center of the first lattice plane. Let the atoms j of the surface plane be located at

$$\mathbf{l}_j = n_{1j}\mathbf{a}_1 + n_{2j}\mathbf{a}_2 \tag{5}$$

then the distance between atom j and the particle p is written

$$r_{pj} = \sqrt{\rho_{pj}^2 + z_{pj}^2} \tag{6}$$

where $\rho_{pj}^2 = x_{pj}^2 + y_{pj}^2$, and x_{pj}, y_{pj}, z_{pj} are the components of the vector

$$\mathbf{r}_{pj} = \mathbf{r}_p - \mathbf{l}_j \tag{7}$$

In this frame the anisotropic part of the potential has the form

$$V_{an}(p;\mathbf{r}_p) = 4\epsilon_{ps} \sum_j \left[\left(\frac{\sigma_{ps}^2}{(\alpha\rho_{pj})^2 + z_{pj}^2} \right)^6 - \left(\frac{\sigma_{ps}^2}{(\rho_j/\alpha)^2 + z_{pj}^2} \right)^3 \right] \tag{8}$$

Here α is a scaling parameter that acts differently on the repulsive and attractive parts and gives the potential its anisotropy between directions in the xy plane and the z axis. In our calculations α was set equal to 0.8, since much smaller values would not be consistent with weakly chemisorbed molecules. The summation in Eqn.(8) is taken over all atoms j of the surface.

The short-range isotropic contribution can, in general, be described as

$$V_{isr}(n,p;\mathbf{r}_p) = -4\epsilon_{ps}\sum_j \frac{C_n(p)\sigma_{ps}^n}{r_{pj}^n} \tag{9}$$

where C_n is a fitting parameter with n being an integer. The scale factors σ_{ps} and ϵ_{ps} are separated for mathematical convenience.

Now that we have described the form of the water-core interactions for the two models we can write down the complete potentials for the two cases. In the first model (A1) we have

$$V_{\mathrm{A1}} = V_{w-cond} + V_{an}(\mathrm{O};\mathbf{r}_{\mathrm{O}}) + V_{isr}(8,\mathrm{O};\mathbf{r}_{\mathrm{O}}) - \sum_{\mathrm{H}} V_{isr}(6,\mathrm{H};\mathbf{r}_{\mathrm{H}}) \tag{10}$$

In the second model (A2) we have

$$V_{\mathrm{A2}} = V_{w-cond} + V_{an}(\mathrm{O};\mathbf{r}_{\mathrm{O}}) + V_{isr}(10,\mathrm{O};\mathbf{r}_{\mathrm{O}}) + \sum_{\mathrm{H}}[V_{an}(\mathrm{H};\mathbf{r}_{\mathrm{H}}) + V_{isr}(10,\mathrm{H};\mathbf{r}_{\mathrm{H}})] \tag{11}$$

Note that in the second model A2, both the oxygen and hydrogen atoms in water interact with the metal atoms through the anisotropic Lennard-Jones potential, and the short-range interaction now has an inverse tenth power dependence. This latter change is needed to describe the atomic polarization under strong electric field near the metal surface. The physical origin of such electrostatic field is the deformation of the electron cloud within a metal [27, 28, 29]. We shall show that model A2 improves the binding energy, the equilibrium distance, and the adsorption via hydrogen atoms over model A1 but at the cost of more complexity.

Following the derivation of Steele [24, 25], the lattice sum in Eqn.(8) is transformed to reciprocal space:

$$V_{an}(p;\mathbf{r}_p) = \frac{8\pi\epsilon_{ps}\sigma_{ps}^2}{A_{\mathrm{cell}}}\left\{\frac{\sigma_{ps}^{10}}{10\alpha^2 z^{10}} - \frac{\alpha^2\sigma_{ps}^4}{4z^4} + \right.$$

$$\sum_{g_j} G(g_j;\mathbf{g}_j\cdot\boldsymbol{\rho})\left[\frac{\sigma_{ps}^{10}}{120\alpha^7}\left(\frac{g_j}{2z}\right)^5 K_5(g_jz/\alpha)-\frac{\alpha^4\sigma_{ps}^4}{2}\left(\frac{g_j}{2z}\right)^2 K_2(\alpha g_jz)\right]\Bigg\} \quad (12)$$

In the above equation, the label p is omitted on the right hand side from ρ and z, A_{cell} is the surface area of a unit lattice cell, $K_m(\xi)$ stands for mth order modified Bessel function of the second kind, and $G(g_j;\mathbf{g}_j\cdot\boldsymbol{\rho})$ includes contributions from all the trigonometric factors $\cos(\mathbf{g}_j\cdot\boldsymbol{\rho})$ with the restriction of g_j = constant.

Analogously the short range component V_{isr} can be written

$$V_{isr}(n,p;\mathbf{r}_p)=$$

$$-\frac{8\pi\epsilon_{ps}\sigma_{ps}^2}{A_{cell}}\left[\frac{C_n(p)}{n-2}\left(\frac{\sigma_{ps}}{z}\right)^{n-2}+\sum_{g_j} G(g_j;\mathbf{g}_j\cdot\boldsymbol{\rho})\frac{\sigma_{ps}^{n-2}}{(n/2-1)!}\left(\frac{g_j}{2z}\right)^{n/2-1}K_{n/2-1}(g_jz)\right] \quad (13)$$

in terms of the same set of geometric factors G. Note that the G factors depend on the symmetry of the lattice plane and are different for (111), (100), and (110) planes.

We conclude with explicit lists of the geometric factors for each of the three main low index planes starting with the square lattice. For the (100) plane where $|\mathbf{a}_1| = |\mathbf{a}_2| = a/\sqrt{2}$ and $A_{cell} = a^2/2$, the lengths of the two-dimensional $\mathbf{g}_j$ vectors in the reciprocal lattice space are given by

$$g_j = \frac{2\pi}{a}\left(g_{j1}^2+g_{j2}^2\right)^{1/2} \quad (14)$$

where a is the lattice constant, g_{j1} and g_{j2} are a set of integers, which satisfy g_j = constant. Accordingly, we write the dot product of $\mathbf{g}_j$ and $\boldsymbol{\rho}$ as

$$\mathbf{g}_j\cdot\boldsymbol{\rho} = \frac{2\pi}{a}(g_{j1}x+g_{j2}y). \quad (15)$$

Straightforward manipulation of Eqns.(14) and (15) leads to the following explicit expressions for the first five leading terms of the corrugation factors G:

$$G(g_1;\mathbf{g}_1\cdot\boldsymbol{\rho}) = \cos\beta_x x+\cos\beta_y y,$$

$$G(g_2;\mathbf{g}_2\cdot\boldsymbol{\rho}) = 2\cos\beta_x x\cos\beta_y y,$$

$$G(g_3;\mathbf{g}_3\cdot\boldsymbol{\rho}) = \cos 2\beta_x x+\cos 2\beta_y y,$$

$$G(g_4; \mathbf{g}_4 \cdot \boldsymbol{\rho}) = 2\left(\cos 2\beta_x x \cos \beta_y y + \cos \beta_x x \cos 2\beta_y y\right),$$

and

$$G(g_5; \mathbf{g}_5 \cdot \boldsymbol{\rho}) = 2 \cos 4\beta_x x \cos 4\beta_y y,$$

corresponding to $g_1 = \beta_x$, $g_2 = \sqrt{2}\beta_x$, $g_3 \doteq 2\beta_x$, $g_4 = \sqrt{5}\beta_x$, and $g_5 = 2g_2$. In the above equations, $\beta_x = \beta_y = 2\sqrt{2}\pi/a$.

The situation for (110) surface is similar, except for $|\mathbf{a}_1| = |\mathbf{a}_2|/\sqrt{2} = a/\sqrt{2}$. Accordingly, equation (14) is replaced by

$$g_j = \frac{2\pi}{a}\left(2g_{j1}^2 + g_{j2}^2\right)^{1/2} \tag{16}$$

which leads to

$$\mathbf{g}_j \cdot \boldsymbol{\rho} = \frac{2\pi}{a}(\sqrt{2}g_{j1}x + g_{j2}y).$$

Since the Fourier series converges relatively slowly at small z for this surface, we keep the first ten terms, corresponding to $g_1 = 2\pi/a$, $g_2 = \sqrt{2}g_1$, $g_3 = \sqrt{3}g_1$, $g_4 = 2g_1$, $g_5 = \sqrt{6}g_1$, $g_6 = 2g_2$, $g_7 = 3g_1$, $g_8 = \sqrt{11}g_1$, $g_9 = 2g_3$, and $g_{10} = 4g_1$. These corrugation components have the form of

$$G(g_1; \mathbf{g}_1 \cdot \boldsymbol{\rho}) = \cos \beta_y y,$$

$$G(g_2; \mathbf{g}_2 \cdot \boldsymbol{\rho}) = \cos \beta_x x,$$

$$G(g_3; \mathbf{g}_3 \cdot \boldsymbol{\rho}) = 2 \cos \beta_x x \cos \beta_y y,$$

$$G(g_4; \mathbf{g}_4 \cdot \boldsymbol{\rho}) = \cos 2\beta_y y,$$

$$G(g_5; \mathbf{g}_5 \cdot \boldsymbol{\rho}) = 2 \cos \beta_x x \cos 2\beta_y y,$$

$$G(g_6; \mathbf{g}_6 \cdot \boldsymbol{\rho}) = \cos 2\beta_x x,$$

$$G(g_7; \mathbf{g}_7 \cdot \boldsymbol{\rho}) = \cos 3\beta_y y + 2 \cos 2\beta_x x \cos \beta_y y,$$

$$G(g_8; \mathbf{g}_8 \cdot \boldsymbol{\rho}) = 2 \cos \beta_x x \cos 3\beta_y y,$$

$$G(g_9; \mathbf{g}_9 \cdot \boldsymbol{\rho}) = 2 \cos 2\beta_x x \cos 2\beta_y y,$$

and

$$G(g_{10}; \mathbf{g}_{10} \cdot \boldsymbol{\rho}) = \cos 4\beta_y y$$

with $\beta_x = g_2$ and $\beta_y = g_1$.

In the case of (111) plane, $|\mathbf{a}_1| = |\mathbf{a}_2| = a/\sqrt{2}$ and $A_{\text{cell}} = \sqrt{3}a^2/2$. The magnitude of $\mathbf{g}_j$ is evaluated by

$$g_j = \frac{4\pi}{\sqrt{3}} \left(g_{j1}^2 + g_{j2}^2 - g_{j1}g_{j2}\right)^{1/2}, \tag{17}$$

which gives $g_1 = 2\beta_y$, $g_2 = \sqrt{3}g_1$, $g_3 = 2g_1$, $g_4 = \sqrt{7}g_1$, $g_5 = 3g_1 \cdots$ with $\beta_x = 2\sqrt{2}\pi/a$ and $\beta_y = 2\beta_x/\sqrt{3}$. For such configuration, the dot product

$$\mathbf{g}_j \cdot \boldsymbol{\rho} = \frac{2\pi}{a} \left[(2g_{j1} - g_{j2})x/\sqrt{3} + g_{j2}y\right], \tag{18}$$

yielding the first five terms in the Fourier series:

$$G(g_1; \mathbf{g}_1 \cdot \boldsymbol{\rho}) = \cos 2\beta_y y + 2\cos\beta_x x \cos\beta_y y,$$

$$\begin{aligned}
G(g_2; \mathbf{g}_2 \cdot \boldsymbol{\rho}) &= \cos 2\beta_x x + 2\cos\beta_x x \cos 3\beta_y y, \\
G(g_3; \mathbf{g}_3 \cdot \boldsymbol{\rho}) &= \cos 4\beta_y y + 2\cos 2\beta_x x \cos 2\beta_y y, \\
G(g_4; \mathbf{g}_4 \cdot \boldsymbol{\rho}) &= 2(\cos 3\beta_x x \cos\beta_y y + \cos 2\beta_x x \cos 4\beta_y y + \cos\beta_x x \cos 5\beta_y y), \\
G(g_5; \mathbf{g}_5 \cdot \boldsymbol{\rho}) &= \cos 6\beta_y y + 2\cos 3\beta_x x \cos 3\beta_y y.
\end{aligned}$$

In most cases, only the first few expansion terms are necessary to achieve sufficient accuracy. However, for some extreme conditions, there may be a need to keep more terms.

3 Results and Discussion

In this section we describe calculations with the two forms of the potential for different low index planes of some fcc metals. In all the calculations, we set $\alpha = 0.8$, which reduces the effective radius for the repulsion and increases the radius for the attraction through inverse dependence in the second term of Eqn. (8), when the projection vector $\boldsymbol{\rho}_{pj}$ is not null. The simple point charge model SPC/E is used to represent the water molecule. Its geometry, partial charges, and Lennard-Jones parameters are used for model A1. For model A2, the Lennard-Jones parameters were replaced by taking the oxygen as a neon atom with $\sigma_{\text{O}} = 0.286$nm, $\epsilon_{\text{O}} = 0.229$kJ/mol [30], and hydrogen as a helium, with $\sigma_{\text{H}} = 0.256$nm, and $\epsilon_{\text{H}} = 0.0845$kJ/mol [31].

The Lennard-Jones parameters for the metals were taken from the literature. Table I lists the potential parameters evaluated from a variety of crystalline state physical properties at a wide-range of temperatures [33, 34] and the lattice constants [30] for a selected set of metals. To get the coupling parameters (so-called mixed Lennard-Jones parameters) needed for the two forms of potential described in the last section we used the parameters just described and the the well-known Kong's combining rules [32]. This limits the number of the fitting parameters to the two Cs in Eqns.(8 - 11), except in the case of Al where there was only one parameter. In passing we comment that since the Lennard-Jones radii and energies used in A2 do not depend on the particular model, readjustment of parameters for other water models that have different geometry and point charges is straightforward.

Reported in Table II are the coefficients for the angular independent, short-range interactions in V_{isr} Eqns.(9 - 11), obtained by a fit to the *ab initio* binding energies of water on Ni(111) [14], Pt(100) [10], and Al(100) [11]. For the case of aluminum, we simplified the calculation further by setting $C_{10}(\mathrm{H}) = 0$. In this study, we define the atop site as the position right above a metal atom, the bridge site as the position above the middle point of the $\mathbf{a}_1$ vector, and the hollow site is the one with a second layer metal atom underneath. There is a complication that we did not consider in our calculations. According to the calculations of Yang and Whitten [14] for Ni, the adsorption energy for the hollow site with no second layer metal atom underneath is 9.59 kJ/mol larger than the one with the atom. We considered this effect to be beyond the scope of the present model and so we took an average value of the two, -28.65 kJ/mol, as the criterion for comparison. It should also be mentioned that all the quantum-mechanical calculation results are based on small clusters, and may depart from the surface results significantly.

Although the fitting procedure is for specific low index faces, the parameters determined are equally applicable to other types of crystallographic structure as well as to discrete atomic layers. This can clearly be seen from Tables III-V where comparisons with results from other potential functions and/or molecular orbital calculations are given. Keep in mind that two assumptions are implicit in the above statement: pair-wise additivity approximation for non-Coulombic interactions and the validity of the combining rule. Also note that the adsorption energies were calculated for a molecular orientation with the oxygen atom closest to the surface ('oxygen atom down') and with the vector bisecting the H-O-H bond angle perpendicular to the interface, and the line connecting the two hydrogen atoms parallel to the x-axis (parallel to $\mathbf{a}_1$). These calculated results are consistent with experimental measurements [9, 35, 36, 37, 38].

According to our calculations, the equilibrium distances between the oxygen atom of the water molecule and the Ni(111) surface at atop, bridge, and hollow sites are, respectively, 0.249, 0.260, 0.261 nm for model A1 and 0.226, 0.240, 0.243 nm for model A2, compared with 0.206, 0.209, 0.210 nm of Yang and Whitten [14]. Both our models predict an equilibrium distance that is too large compared to the *ab initio* calculations. Model A2 is marginally 'better' than A1 in yielding the bond distances that are smaller and closer to the cluster calculation.

According to the calculation of Yang and Whitten [14], the adsorption energy of water on Ni(111) surface is shifted upward by 5.02 kJ/mol when the molecule on the atop site rotates about the C_{2v} axis by 90° so the H-H line becomes parallel to the y-axis. In our model, the energy difference turns out to be much smaller since the distances from the hydrogen nuclei to the nearest Ni atom remain the same after the rotation. It seems that the energy shift observed by Yang and Whitten arises from some binding contributions absent in the present model.

It is informative to examine the energy variation with respect to ϕ which is defined as the angle between the molecular dipole moment vector and the z axis normal to the surface. In particular, rotating the water molecule on the Ni(111) surface (keeping z_O fixed at the equilibrium distance) by $\phi = 49.75°$ in the xz plane increases the binding energy to -4.19 kJ/mol for model A1 and to -9.52 kJ/mol for model A2 at atop site, to -25.24 kJ/mol and 18.51 kJ/mol at the bridge site, and to 4.83 kJ/mol and -15.37 kJ/mol at the hollow site. On the other hand, the value calculated by Yang and Whitten [14] for the atop site at $\phi = 52.25°$ is 25.10 kJ/mol. There is a 5° difference in the H-O-H bond angle of the SPC/E model compared to the geometry of water in the *ab initio* cluster. However we have chosen ϕ such that one of our O-H bonds makes the same angle relative to the z axis as in the Yang-Whitten calculation. Clearly our relatively simple model underestimates the rotational barrier.

By allowing the molecular dipole to change its direction along the yz plane, using ψ to measure the angle between the dipole vector and the surface normal, we are able to study the binding energy variation upon molecular tilt.

Successively tilting the water molecule in increments of 10° from the surface normal ($\psi = 0$) changes the binding energy at the top site to -43.82 ($\psi = 10°$), -42.20 ($\psi = 20°$), -39.45 ($\psi = 30°$), -35.51 ($\psi = 40°$), -30.25 ($\psi = 50°$), -23,57 ($\psi = 60°$) kJ/mol for model A1 and to -44.32, -44.02, -43.50, -42.77, -41.76, -40.32 kJ/mol for model A2. By comparison, the corresponding values of Yang and Whitten were: -47.28, -48.12, -48.12, -45.19, -41.00, -35.98 kJ/mol. The energies computed from the simple models show a monotonic increase, the quantum calculation result displays a minimum around $\psi = 20°$ to 30°. These discrepancies should not affect the computer simulation results significantly since they only affect the water in contact with the surface and decrease rapidly with increasing distance z.

The Lennard-Jones parameters obtained from thermodynamic data suggest that Cu, Ag, Au, and Ni form a single class, and Pt yet another with stronger binding. Using the fitting coefficients of Ni, we are able to predict the energies for adsorption on copper surfaces. The results are given in Table VI, and show that the predicted binding energy of water molecule right above a metal atom of Cu(100), -38.70 kJ/mol at 0.251 nm for model A1 and -38.95 kJ/mol at 0.228 nm for model A2, is in accord with the *ab initio* results of Ribarsky and co-workers [12], namely -36.66 kJ/mol at 0.220 nm.

All the potential surfaces depicted in Tables III-VI indicate a preference for water to adopt orientations in which water dipole moment points away from the interface and the oxygen sits down on the surface with the on top site being the site with greatest binding energy. If more experimental data were available the potentials described here could be further refined.

Using the parameters reported in Tables I and II, we plot the potential energy curves calculated from the analytical formulas derived in Section 2 for one oriented water molecule adsorbed at different sites on low index faces of platinum. The results are shown by the curves in Figures 1-3. For comparison, we also plot the potential energies (data points) obtained from the direct summation of pair-wise interaction. Both sets of calculations explicitly included the top two layers of metal surface atoms and approximated the remainder of the crystal by means of the 9-3 potential that comes from treating the remaining half space in the continuum limit. As can be seen there, the agreement between these two sets of computations is excellent. The largest deviations hardly visible in the plots occur when the particle-wall distance is very short. Since the use of the transformed form of the potential energy is computationally much more economical, direct summation of pair-wise interaction is not necessary in computer simulations unless inclusion of the thermal motions of the metal atoms is desired. In Figs. 1-3, about 75% of the adsorption energy on atop site comes from the interaction with the nearest metal atom. For bridge site, on the other hand, the contribution from the two nearest neighbors is about 65%. By comparing the potentials at distances greater than 0.35 nm in Figures 1-3 we see that the corrugation potential decays very rapidly with distance z from the metal surface. However if the first layer of water is strongly bound in an ordered array then effects of corrugation will be felt further out.

When angle dependence of the potential is turned off ($\alpha = 1$ and $C_n(p) = 0$), the top site becomes the site of weakest binding. This is shown for the Pt(111) surface and model A2 in Figure 4. Figure 4 shows how anisotropy is important in lowering energy of the top site and in decreasing the metal-oxygen bond distance. As mentioned above, introduction of the angular dependent, short-range interactions to represent chemical bonding is essential for mimicking water adsorption on metallic surfaces. The Lennard-Jones potential function does not produce correct preferential adsorption site. By adding the angular dependent, short-range interactions, the potential well for atop site deepens and shifts towards small z, while for the bridge and hollow sites the influence is just opposite. This reverses the preference order for adsorption energies. The contribution from image interactions is also shown in Figure 4.

In Figure 5 we plot the total energy of H_2O-Pt(100) system versus the O-surface separation. The molecular orientation is such that one O-H bond vector is perpendicular to the horizontal surface plane with one hydrogen pointing directly at the surface. The other O-H bond lies in the xz plane pointing away from the surface at an oblique angle. This mimics the situation where chemisorption is through the hydrogen atom. For such a configuration, we obtain the binding energies of -26.11 kJ/mol at 0.334 nm for the atop site, -15.82 kJ/mol at 0.349 nm for the bridge site, and -13.38 kJ/mol at 0.352 nm for the hollow site (model A2). The corresponding values from the molecular orbital calculation of Holloway and Bennemann [10] are -24.18 kJ/mol at 0.265 nm for the first position and -5.94 kJ/mol at 0.268 nm for the third position. Model A1 does not predict any significant adsorption via hydrogen atom. Note that the shift in minima for oxygen versus hydrogen down is approximately 0.1 nm. This is the shift observed by Toney et al [4] in the experiments with bulk water next to a silver surface when the electric field is reversed. This is an added reason for adopting potentials with the form described here.

Compared with other analytical potential functions, the present one is physically more meaningful. It contains a small enough number of fitting parameters to not overly prejudice the physics. In addition, the functional form is universal for studying water adsorption on various metal surfaces and can be directly used for systems in which the metal atoms are explicitly taken into account. As new experimental or theoretical data on the adsorption energy, etc., becomes available, it will be very easy to modify the potential function and refine the parameters. One possible channel of improvement of the present model is to add non-additive interactions such as electric polarizations or other many-body interactions explicitly. Work on modifying the potentials to include electric polarization is in progress.

4 Acknowledgment

This work was supported in part by the Office of Naval Research. SBZ is grateful to Dr. John A. Barker for helpful discussions.

References

[1] P. A. Thiel and T. E. Madey, Surf. Sci. Rep. 7, 211 (1987).

[2] A. E. Russell, A. S. Lin and W. E. O'Grady, J. Chem. Soc. Faraday Trans. 89, 195 (1993).

[3] C. A. Melendres, B. Beden, G. Bowmaker, C. Liu and V. A. Maroni, Langmuir 9, 1980 (1993).

[4] M. F. Toney, J. N. Howard, J. Richer, G.L. Borges, J. G. Gordon O. R. Melroy, D. G. Weisler, D.Yee, and L. B. Sorensen, The distribution of water molecules at the silver(111)-electrolyte interface, submitted to Nature 11/1993.

[5] E. Spohr and K. Heinzinger, Chem. Phys. Lett. 123 (1986) 218.

[6] N. G. Parsonage and D. Nicholson, J. Chem. Soc. Faraday Trans. II 82, 1521 (1986).

[7] N. G. Parsonage and D. Nicholson, J. Chem. Soc. Faraday Trans. II 83, 663 (1987).

[8] A. A. Gardner and J. P. Valleau, J. Chem. Phys. 86, 4171 (1987).

[9] G. B. Fisher and J. L. Gland, Surf. Sci. 94, 446 (1980).

[10] S. Holloway and K. H. Bennemann, Surf. Sci. 101, 327 (1980).

[11] J. E. Müller and J. Harris, Phys. Rev. Lett. 53, 2493 (1984).

[12] M. W. Ribarsky, W. D. Luedtke, and U. Landman, Phys. Rev. B 32, 1430 (1985).

[13] C. W. Bauschlicher, Jr., J. Chem. Phys. 83, 3129 (1985).

[14] H. Yang and J. L. Whitten, Surf. Sci. 223, 131 (1989).

[15] E. Spohr and K. Heinzinger, Ber. Bunsenges. Phys. Chem. 92, 1358 (1988).

[16] E. Spohr, J. Phys. Chem. 93, 6171 (1989).

[17] K. Forster, K. Raghavan, and M. Berkowitz, Chem. Phys. Lett. 162, 32 (1989).

[18] K. Raghvan, K. Foster, K. Motakabbir, and M. Berkowitz, J. Chem. Phys. 94, 2110 (1991).

[19] J. I. Siepmann and M. Sprik, Surf. Sci. Lett. 279, L185 (1992).

[20] F. H. Stillinger and T. A. Weber, Phys. Rev. B 31, 5262 (1985).

[21] J. A. Barker and C. T. Rettner, J. Chem. Phys. 97, 5844 (1992).

[22] N. N. Avgul and A. V. Kiselev, in *"Chemistry and Physics of Carbon"*, Vol. 6 (Dekker: New York, 1970).

[23] J. Hove and J. A. Krumhansl, Phys. Rev. 92, 569 (1953).

[24] W. A. Steele, Surf. Sci. 36, 317 (1973).

[25] W. A. Steele, *"The Interaction of Gases with Solid Surfaces"*, (Pergamon Press: Oxford, 1974).

[26] J. D. Jackson, *"Classical Electrodynamics"* (John Wiley & Sons: New York, 1962).

[27] B. Mrowka and A. Recknagel, Physik, Z. 38, 758 (1937).

[28] J. C. P. Mignolet, Disc. Faraday Soc. 8, 105 (1950).

[29] J. H. Kaspersma, Ph.D. Thesis, (Catholic Univ. of Nijmegen: Nethelands, 1972).

[30] *American Institute of Physics Handbook*, Third Edition (McGraw-Hill Book Company: New York, 1982).

[31] J. O. Hirschfelder, C. F. Curtiss, and R. B. Bird, *"Molecular Theory of Gas and Liquids"* (John Wiley and Sons: 1954).

[32] C. L. Kong, J. Chem. Phys. 59, 2464 (1973).

[33] T. Haliciogũlu and G. M. Pound, Phys. Stat. Sol. A 30, 619 (1975).

[34] C. Kittel, *"Introduction to Solid State Physics"*, Sixth Edition (John Wiley and Sons: New York, 1986).

[35] H. Ibach and S. Lehwald, Surf. Sci. 91, 187 (1980).

[36] T. E. Madey and F. P. Nezter, Surf. Sci. 117, 549 (1982).

[37] F. P. Nezter and T. E. Madey, Surf. Sci. 127, L102 (1983).

[38] R. H. Stulen and P. A. Thiel, Surf. Sci. 157, 99 (1985).

Table I Potential parameters [33] and lattice constants [30] for various metals.

Metals	ϵ (kJ/mol)	σ (nm)	a (nm)
Al	37.84	0.262	0.405
Cu	39.49	0.234	0.362
Ni	50.14	0.228	0.352
Pt	65.77	0.254	0.392

Table II Potential parameters.

Metals	C_{10} (O)	C_{10} (H)	C_8 (O)	C_6 (H)
Al	1.56	0	2.16	4.4
Ni	1.195	0.8	1.603	3
Pt	1.25	1.2	1.331	1.35

$\alpha = 0.8$, $\sigma_w = 0.316$ nm, $\sigma_O = 0.286$ nm, $\sigma_H = 0.256$ nm, $\epsilon_w = 0.650$ kJ/mol, $\epsilon_O = 0.229$ kJ/mol, $\epsilon_H = 0.0845$ kJ/mol.

Table III Adsorption energies of water on nickel surfaces (in units of kJ/mol).

	A1	A2	YW	SS
(100) A	-43.79	-43.76	-	-49.0
(100) B	-27.68	-28.56	-	-
(100) H	-22.08	-23.65	-	-
(110) A	-43.12	-42.85	-	-55.9
(110) B	-40.46	-27.08	-	-
(110) H	-26.77	-18.90	-	-
(111) A	-44.36	-44.43	-44.35	-43.5
(111) B	-29.74	-29.85	-29.71	-28.3
(111) H	-28.69	-28.28	-28.65	-27.4

A: A-top; B: Bridge site; H: Hollow site; ZP: Present work; YW: Ref. [14]; SS: Ref. [19]; Same for Tables IV-VI.

Table IV Adsorption energies of water on aluminum surfaces (in units of kJ/mol).

	A1	A2	MH
(100) A	-51.06	-51.27	-51.14
(100) B	-22.69	-23.12	-24.12
(100) H	-15.17	-17.86	-14.47
(110) A	-51.32	-50.58	-
(110) B	-22.80	-22.01	-
(110) H	-8.36	-13.89	-
(111) A	-50.78	-51.27	-
(111) B	-24.29	-24.08	-
(111) H	-22.83	-22.39	-

MH: Ref. [11]

Table V Adsorption energies of water on platinum surfaces (in units of kJ/mol).

	A1	A2	SS	SH	RFMB	HB	FRB
(100) A	-48.25	-48.23	-43.3	-35.7	-	-48.25	-39.5
(100) B	-33.18	-28.88	-22.2	-16.3	-	-	-22.0
(100) H	-27.94	-23.00	-20.7	-12.1	-	-27.94	-8.2
(110) A	-46.03	-47.28	-	-	-	-	-
(110) B	-30.96	-27.39	-	-	-	-	-
(110) H	-20.72	-17.90	-	-	-	-	-
(111) A	-49.74	-48.97	-	-	-40.7	-	-
(111) B	-35.67	-30.17	-	-	-26.1	-	-
(111) H	-34.57	-28.12	-	-	-23.9	-	-

SH: Ref. [16]; RFMB: Ref. [18]; HB: Ref. [10]; FRB: Ref. [17].

Table VI Adsorption energies of water on copper surfaces (in units of kJ/mol).

	A1	A2	RLL
(100) A	-38.70	-38.95	-36.66
(100) B	-23.95	-25.11	-
(100) H	-18.97	-20.74	-
(110) A	-38.20	-38.16	-
(110) B	-23.25	-23.85	-
(110) H	-12.91	-16.78	-
(111) A	-39.12	-39.52	-
(111) B	-25.67	-26.19	-
(111) B	-24.73	-24.76	-

RLL: Ref. [12]

Figure Caption

Fig. 1 Water-Pt(100) potential (model A2) as a function of distance of oxygen atom from surface plane. The molecule lies in y = constant plane with dipole moment vector parallel to surface normal and oxygen atom down. Symbols: direct sums of pair-wise energy. Curves: Fourier series expansion.

Fig. 2 Water-Pt(110) potential (model A2) as a function of distance of oxygen atom from surface plane. The molecule lies in y = constant plane with dipole moment vector parallel to surface normal and oxygen atom down. Symbols: direct sums of pair-wise energy. Curves: Fourier series expansion.

Fig. 3 Water-Pt(111) potential (model A2) as a function of distance of oxygen atom from surface plane. The molecule lies in y = constant plane with dipole moment vector parallel to surface normal and oxygen atom down. Symbols: direct sums of pair-wise energy. Curves: Fourier series expansion.

Fig. 4 Water-Pt(111) potential without anisotropic and short-range isotropic terms. The potential is a sum of the conventional 12-6 Lennard-Jones interaction and the Coulomb interaction between real and image charges. The Coulombic image potential is also plotted separately to show its weak z dependence. The molecule lies in y = constant plane with dipole moment vector parallel to surface normal and oxygen atom down.

Fig. 5 Water-Pt(100) potential (model A2) with H atom down. The potential is plotted as a function of distance of oxygen atom from the surface plane. The molecule lies in y = constant plane with one O-H bond perpendicular to the surface. Note shift in minima by approximately 0.1 nm and reduced binding energies compared to the oxygen atom down orientation shown in Figure 1.

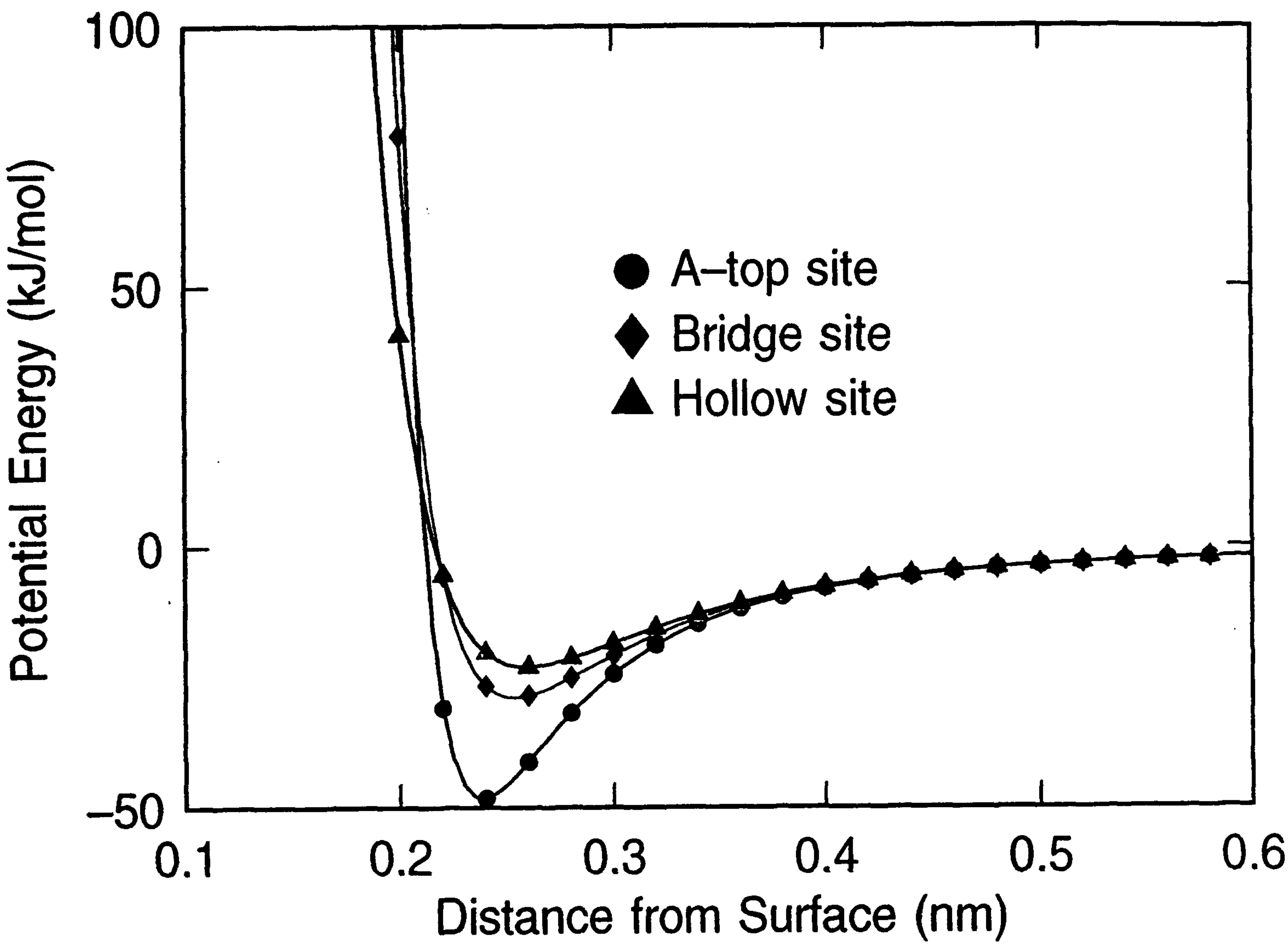

Fig. 1 Water–Pt(100) interaction

Symbols: direct sums of pair–wise energy

Curves: Fourier series expansion of energy

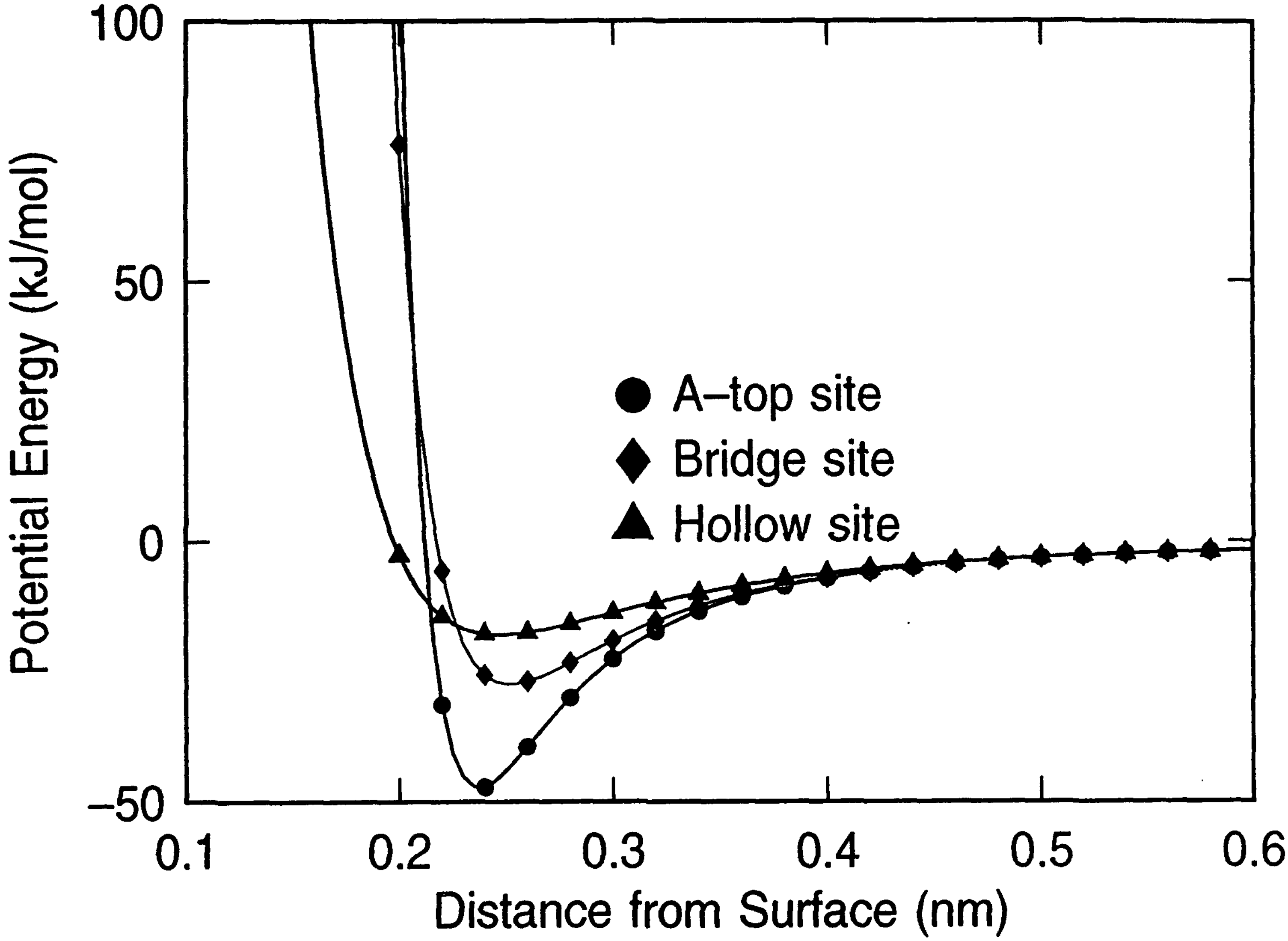

Fig. 2 Water–Pt(110) interaction
Symbols: direct sums of pair–wise energy
Curves: Fourier series expansion of energy

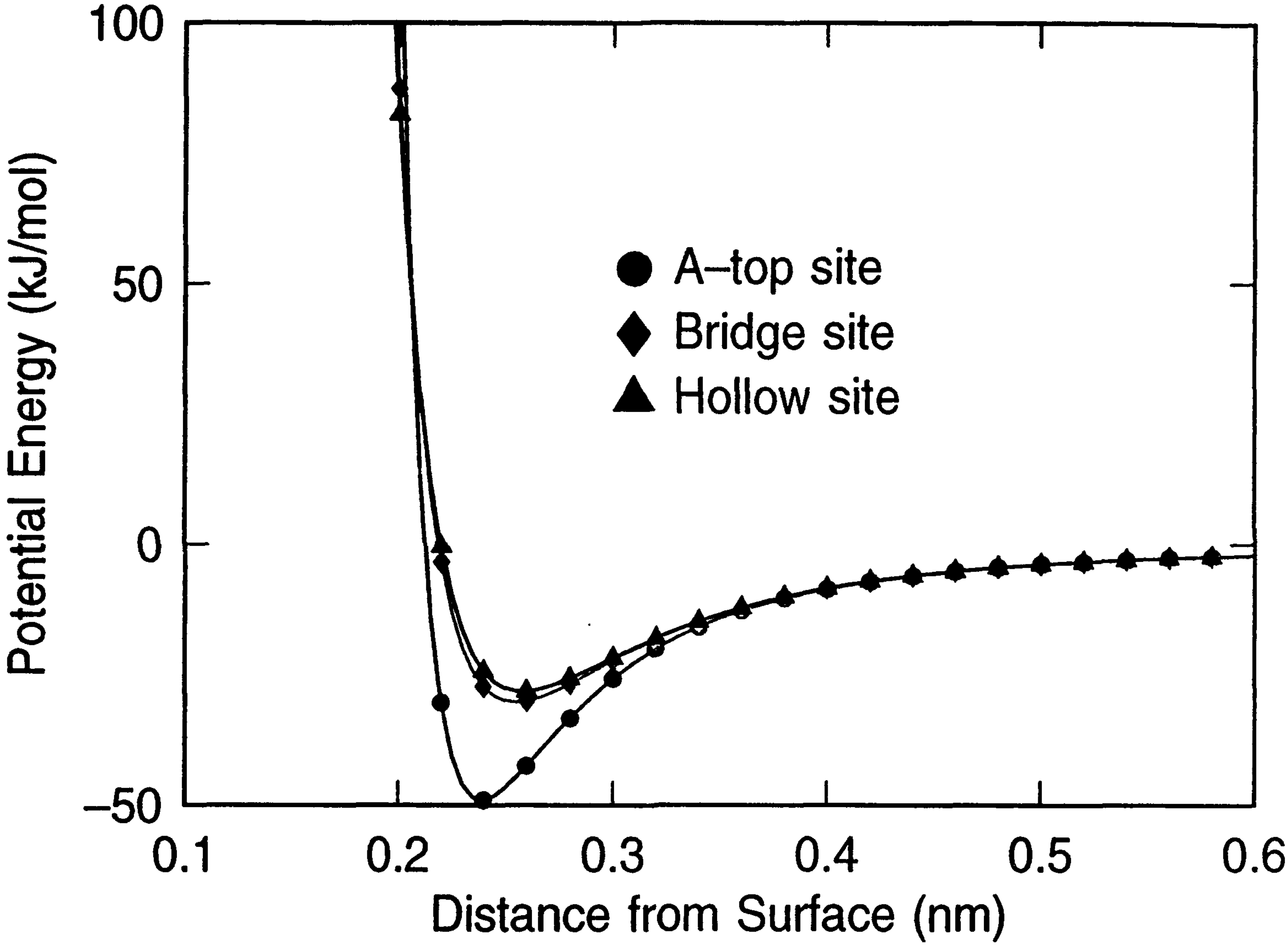

Fig 3 Water–Pt(111) interaction
Symbols: direct sums of pair–wise energy
Curves: Fourier series expansion of energy

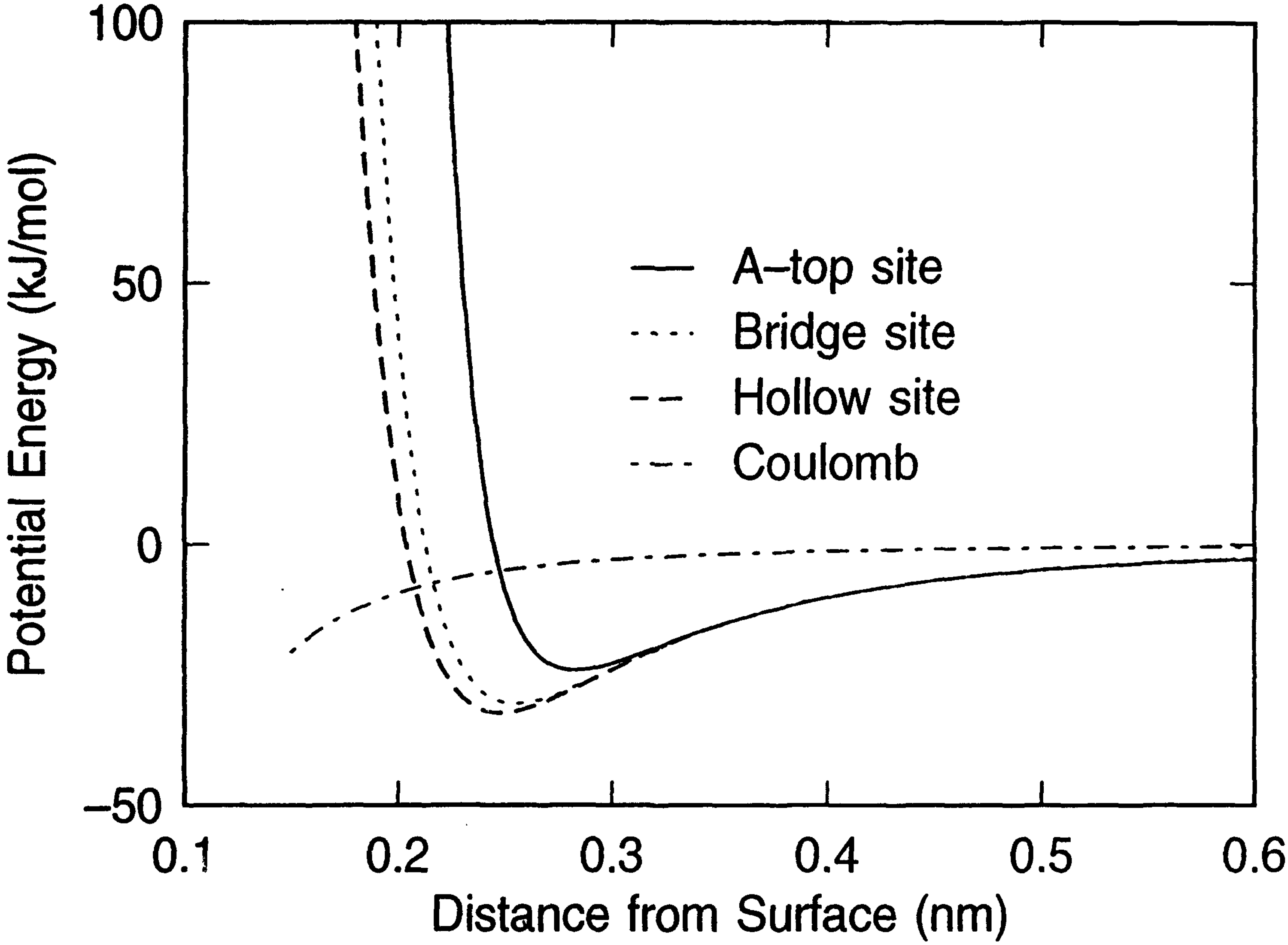

Fig 4 Water–Pt(111) interaction
(12–6 Lennard–Jones & Coulomb)

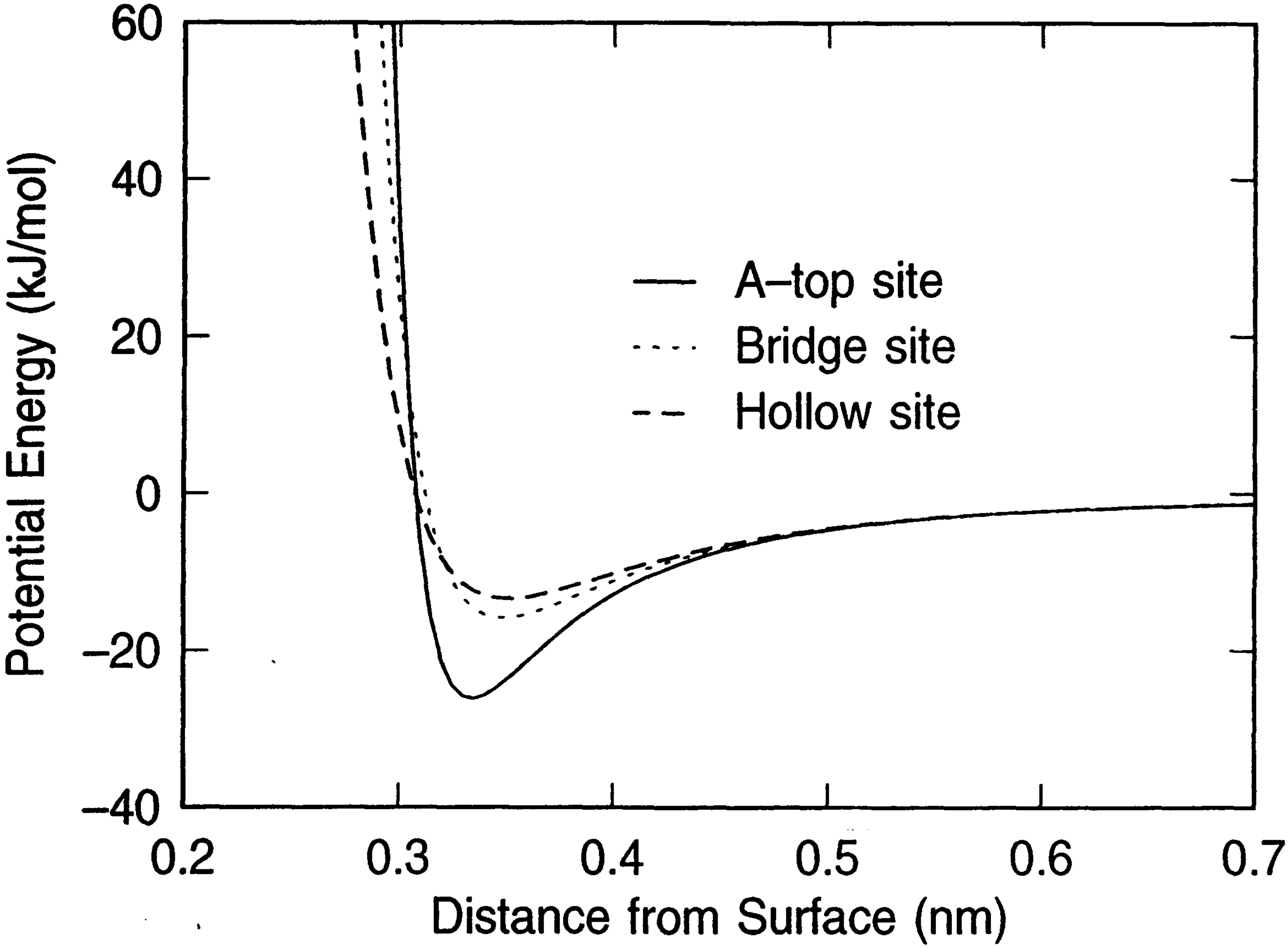

Fig. 5 Water–Pt(100) interaction
Adsorbed via hydrogen